Differential elastic scattering cross sections of 22.1-keV x rays by elements in the range $22 \leqslant Z \leqslant 82$

A. C. Mandal,[1] D. Mitra,[2] M. Sarkar,[2,*] and D. Bhattacharya[2]
[1]*Department of Physics, University of Burdwan, Burdwan 713 104, India*
[2]*Saha Institute of Nuclear Physics, 1/AF, Bidhannagar, Kolkata 700064, India*
(Received 27 September 2001; published 7 October 2002)

Elastic scattering cross sections of 22.1-keV x rays by the elements Ti, V, Fe, Ni, Cu, Zn, Zr, Nb, Mo, Pd, Cd, In, Sn, Sm, Gd, Dy, Er, Yb, Au, and Pb have been measured at 90° with an overall error of 8–10 %. The 22.1-keV x rays were obtained from a Ag foil used as a secondary target in an x-ray fluorescence setup. Experimental cross sections have been compared with the nonrelativistic form factors (NFF), relativistic form factors, modified relativistic form factor (MRFF), relativistic form factor with anomalous scattering correction (RFFASF), modified relativistic form factor with anomalous scattering correction (MRFFASF), and the *S* matrix calculations. For low *Z* elements, experimental values are better represented by *S* matrix, RFFASF, and MRFFASF. For the elements Nb, Mo, and Pd whose *K* shell binding energies are very close to the exciting energy, *the data are higher than all of the theoretical predictions*. For higher *Z* elements, NFF and MRFF give a better agreement with the present data.

DOI: 10.1103/PhysRevA.66.042705 PACS number(s): 32.80.Cy

I. INTRODUCTION

Interaction of photons with matter is one of the most fundamental and basic fields in physics where various experimental as well as theoretical investigations are being carried out till today. Among the four main interactions of photons with matter, e.g., (1) photoelectric process, (2) inelastic scattering, (3) elastic scattering, and (4) pair production, we shall be dealing here with the elastic scattering only. In elastic scattering, the incident photon is deflected but retains the same energy with which it was incident on the target. The contributions to this elastic scattering may come either from (i) the bound electrons, whence the process is called Rayleigh scattering, or from (ii) the nucleus. There are three distinct modes for elastic scattering of photons from the nucleus, e.g., (a) nuclear Thomson scattering, (b) nuclear resonance scattering, and (c) virtual pair creation in the field of the screened nucleus which is known as Delbrück scattering. The nuclear Thomson scattering is dominant when the incident photon energy is $\approx$100 keV, while nuclear resonance scattering and Delbrück scattering play significant roles only at energies beyond 1 MeV. In the energy range of our interest ($E = 22.1$ keV) the Rayleigh scattering would be the predominant mode.

Around 1906, Thomson, after studying the scattering of photons by electrons, proposed his scattering cross section formula for the elastic scattering of photons by an isolated charged particle. Subsequently the form factor (FF) approximation was classically derived as a correction factor to the Thomson elastic scattering cross section and is still used today mainly due to its simplicity. In this approximation, the scattering is considered to be due to a charge distribution instead of a point charge. The differential scattering cross section is then written as

$$\frac{d\sigma}{d\omega} = \frac{d\sigma_T}{d\omega}|f(q)|^2 \tag{1}$$

$$= r_0^2(1+\cos^2\theta)|f(q)|^2, \tag{2}$$

where $d\sigma_T/d\omega$ is the Thomson elastic cross section at an angle θ, covering a solid angle of $d\omega$, $r_0 (= e^2/mc^2)$ is the classical electron radius, $f(q)$ is the FF corresponding to the momentum transfer of

$$hq = 2\left(\frac{h\omega}{c}\right)\sin(\theta/2), \tag{3}$$

and ω is the angular frequency of the incident radiation. This type of cross section calculation is done for a free atom or an ion considering a spherically symmetric electron charge distribution and so no chemical or matrix effects are included in such calculations. This form factor approximation is valid for photon energies much higher than the binding energy of the electron and at large scattering angles.

Extensive calculations of both the nonrelativistic (NFF) and relativistic (RFF) form factors have been done by Hubbell *et al.* [1] and Hubbell and Øverbø [2]. The relativistic calculation has further been improved by incorporating the binding energy of the electron [3]. Values calculated from this latter modification, called modified relativistic form factors (MRFF), are also available in tabular form. The FF approximation, as has been mentioned earlier, is a high-energy approximation. When the energy of the incident photon is close to the absorption edge of an element, the FF approximation fails to predict the experimental results. At such energies, there are strong interference effects due to the spatial distribution of the electrons in an ordered structure. In order to extend the FF approximation towards lower energies, an anomalous scattering factor (ASF) has been introduced so that

$$F(q) = f(q) + f' + if'',$$

*Corresponding author. Email address: mano@anp.saha.ernet.in

where f' is a real number representing the dispersion effect and f'' is an imaginary number representing the absorptive part of the dispersion effect. Investigations on the form of f' and f'' have been done by many groups [4–7].

However, the most successful approach in this field as of now, has been the second ordered perturbation theory, put forward by Brown and Meyers [8] and subsequently refined by Johnson and Cheng [9] and Kissel, Pratt, and Roy [10] using the *S* matrix (SM) formalism. This state-of-the-art calculation contains within it the high-energy form factor, the forward angle energy dependent anomalous scattering factor and goes beyond these approximations to predict reasonable cross sections at all scattering angles and energies. The only practical problem with the SM formalism is the large computation time. However, with the tremendous advancement in the speed of modern machines, such SM calculations are now routine and the results are available through Internet.

Measurements on elastic scattering cross sections have recently been reviewed by Kane *et al.* [11], Roy, Kissel, and Pratt [12], and Bradley, Goncalves, and Kane [13]. It has been reported that there are very few measurements on elastic scattering cross sections in the x-ray energy range and most of them are with gamma rays of energy 59.5 keV or above emitted from an Am^{241} or other radioactive sources. Measurements in the x-ray energy range $E \leqslant 40$ keV are quite sparse and to the best of our knowledge, the groups who have used x-ray energies in their scattering experiments are Shahi *et al.* [14], Elyaseery *et al.* [15], Garg *et al.* [16], Tirsell, Slivinsky, and Ebert [17], Rao, Cesareo, and Gigante [18,19], Smend *et al.* [20], Jung *et al.* [21], and Bui and Milazzo [22].

When elastic scattering cross sections are plotted against scattering angle it is observed that in the region 100°–180°, the value of the scattering cross section is almost constant but in the forward angle the curve is very steep. The flat and steep region meet at around 90° and so a measurement at 90° would be quite revealing. With the modified version of our earlier x-ray tube based x-ray fluorescence system [23,24], we have measured the differential elastic scattering cross sections of Ti, V, Fe, Ni, Cu, Zn, Zr, Nb, Mo, Pd, Cd, In, Sn, Sm, Gd, Dy, Er, Yb, Au, and Pb with 22.1-keV photon at 90°. To the best of our knowledge, there exits only one such set of measurements [22] with this combination of energy and angle. Our particular choice of this energy for the present measurement stems mainly from the fact that (a) with our set of targets, we would be able to investigate the so called edge effect with Nb ($E_k = 18.9986$ keV), Mo ($E_k = 19.9995$ keV), and Pd ($E_k = 24.3503$ keV) and (b) in most of the x-ray fluorescence laboratories, the exciting source is either ^{109}Cd ($E_{K\alpha} = 22.1$ keV) or ^{241}Am ($E_\gamma = 59.54$ keV). In x-ray fluorescence analysis, the scattered peaks are often used (i) to compensate for the matrix effect [25], (ii) for nondestructive analysis of elemental composition of complex materials [26], (iii) to obtain the concentration of lower *Z* element not observable through characteristic x-ray peak analysis [27].

The importance of acquiring new scattering data is twofold. First, data are needed in order to differentiate between the relative efficacies of various theoretical models and obtain a deeper understanding of photon scattering from atoms. Second, such elastic scattering cross sections have wide applications in (1) obtaining information on the structure of atoms and molecules, (2) in medical diagnostics and imaging, (3) in shielding calculations, (4) in food processing industry, and (5) in aviation security.

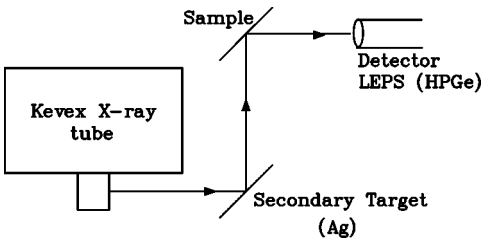

FIG. 1. A schematic diagram of the present experimental setup for the scattering experiment.

II. EXPERIMENT

A 60 W Kevex x-ray tube with a W anode was used as the main x-ray source. Using the geometry as shown in Fig. 1, a silver foil of thickness 0.0264 g/cm^2 was used as a secondary target. Spectroscopically pure foils of Ti, V, Fe, Ni, Cu, Zn, Zr, Nb, Mo, Pd, Cd, In, Sn, Sm, Gd, Dy, Er, Yb, Au, and Pb (shown in Table I with their specifications) have been used as targets. Characteristic and scattered x-rays were detected with an ORTEC LEPS (HPGe) detector placed in a position where the bremsstrahlung intensity was minimum [23]. The resolution of the detector was 170 eV at 5.9 keV. The HPGe detector was fitted with a collimator made from graded shielding of lead, copper, and aluminum with an entrance aperture of 13 mm and exit aperture of 8 mm. The x-ray tube was run at 40 kV with a current of 0.2 mA. Two typical spectra of Fe and Pb are shown in Fig. 2. As can be seen from Fig. 2, the elastically scattered peaks from K_α and K_β are well separated from the inelastically scattered peaks. Accumulation of the spectra continued till the integrated counts under the elastically scattered K_α peak without background was roughly 10 000. The maximum and minimum count rates were 1100 and 650/s, respectively. The time required for such a single run varied from 1 to 3 h. A few runs were repeated with the same preset time and the integrated peak counts were found to be well within the error limits.

The differential elastic scattering cross section at a particular angle θ (here $\theta = 90°$) was then obtained using the relation

$$\left(\frac{d\sigma}{d\Omega}\right)_{\rm el} = \frac{N_{\rm el}}{4\pi I_0 G \varepsilon_{\rm el} m \beta}, \tag{4}$$

where $N_{\rm el}$ is the number of counts per second under the elastic peak, I_0 is the incident flux, G is the geometry factor between the detector and the target, $\varepsilon_{\rm el}$ is the efficiency of the HPGe detector at the elastic peak energy, m is the areal density of the target in g/cm^2 as quoted by the companies, and β is the absorption correction factor for the incident and elastically scattered radiation inside the target and is evaluated using the relation (6).

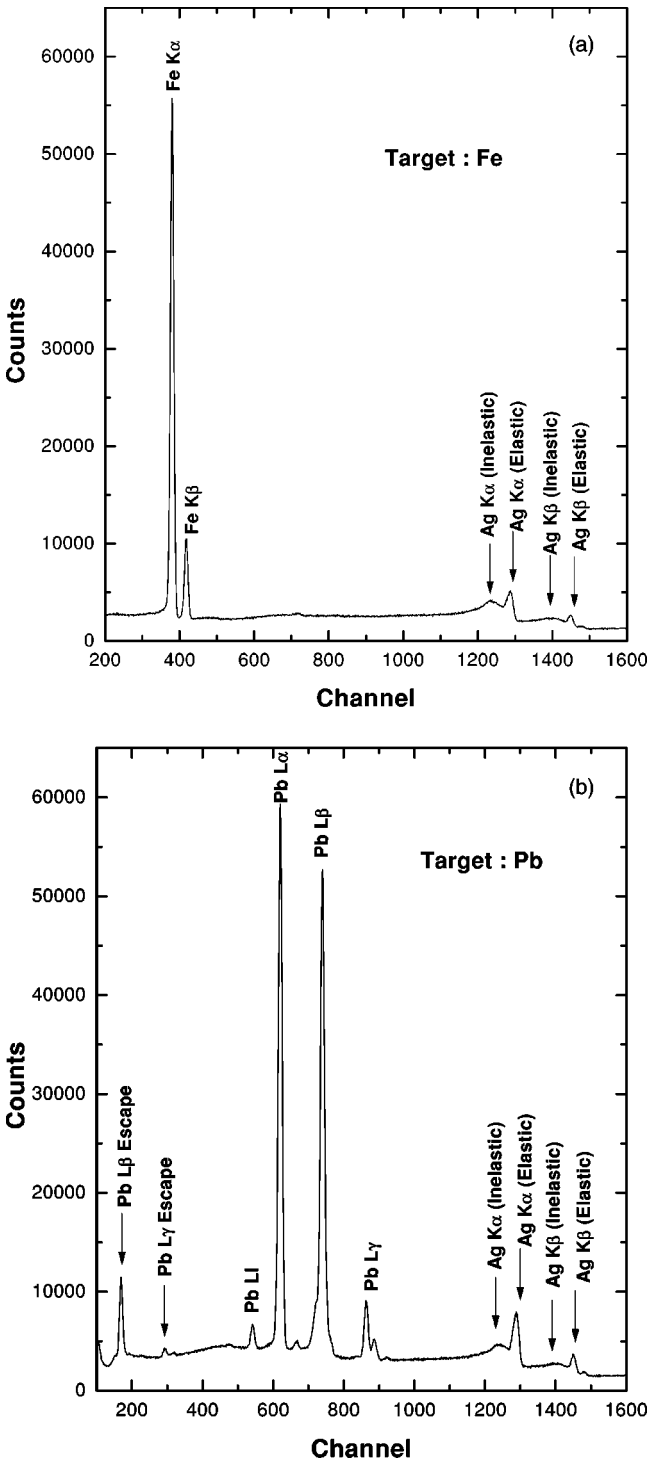

FIG. 2. (a) The full spectrum of Fe target excited by 22. 1-keV x rays obtained from a Ag foil used as a secondary target, (b) same for Pb.

The term $I_0 G\varepsilon$ which includes incident flux, geometry factor, and the absolute efficiency of the detector was determined using the K_α and K_β line intensities of some elemental foils (shown in Table II) with known fluorescence cross sections. The expression used is

$$I_0 G\varepsilon = \frac{N_x}{\sigma m \beta}, \tag{5}$$

TABLE I. Targets used with their thicknesses and corresponding β values.

Element (Z)	Thickness (g/cm^2)	β
Ti (22)	0.0454	0.5149
V (23)	0.0152	0.7631
Fe (26)	0.0178	0.6397
Ni (28)	0.0064	0.8097
Cu (29)	0.0062	0.8058
Zn (30)	0.0535	0.2324
Zr (40)	0.3200	0.0199
Nb (41)	0.0200	0.2873
Mo (42)	0.0120	0.3749
Pd (46)	0.0150	0.7701
Cd (48)	0.0432	0.4684
In (49)	0.0320	0.5375
Sn (50)	0.0090	0.8195
Sm (62)	0.0754	0.1531
Gd (64)	0.1974	0.0540
Dy (66)	0.1067	0.0918
Er (68)	0.0905	0.0986
Yb (70)	0.1744	0.0472
Au (79)	0.0537	0.1092
Pd (82)	0.0150	0.3346

where σ is the the fluorescence cross section of the element used as a target, N_x is the peak integral under the $K_{\alpha,\beta}$ peak, m is the thickness of the target in g/cm^2, and β is the absorption correction factor both for the incident and the fluorescent x-rays. The value of β can be obtained using the relation

$$\beta = \frac{1-\exp[-(\mu_{\text{in}}/\sin\psi_1 + \mu_{\text{em}}/\sin\psi_2)]m}{[\mu_{\text{in}}/\sin\psi_1 + \mu_{\text{em}}/\sin\psi_2]m}, \tag{6}$$

where μ_{in} and μ_{em} are the total mass attenuation coefficient of the incident and emergent x rays obtained from XCOM

TABLE II. Details of the targets for the determination of $I_0 G\varepsilon$.

Element (Z)	Thickness (g/cm^2)	K x-ray energy (keV) K_α	K_β
Fe (26)	0.0178	6.40	7.06
Ni (28)	0.0064	7.48	8.26
Cu (29)	0.0062	8.05	8.91
Zn (30)	0.0535	8.64	9.57
Zr (40)	0.3200	15.78	17.67
Nb (41)	0.0200	16.62	18.62
Mo (42)	0.0120	17.45	19.61
Ag (47)	0.0264	22.16	24.94
Cd (48)	0.0432	23.17	
In (49)	0.0320	24.21	

[28], ψ_1 and ψ_2 are the incident and emergent angle, respectively (each equals 45°). The β values for different foils are shown in Table I.

To check the reproducibility of measurements, runs for two targets were repeated with a time gap of a few days. The readings were found to be within the errors. The K shell photoelectric cross section, fluorescence yields ω_k, and the ratio of K_α to K_β were taken from Scofield [29], Krause [30], and Salem, Panossian, and Krause [31], respectively. With a Ag foil as the secondary target, elements up to Mo could be excited. To extend the value of $I_0 G\varepsilon$ beyond the energies of K_α and K_β of Mo (17.45 and 19.61 keV, respectively) the Ag foil was replaced with a pellet of potassium iodide. Iodine K_α and K_β energies (28.61 and 32.29 keV, respectively) were high enough to excite the K x-rays from Ag, Cd, and In. To normalize these readings with the earlier set, a few of the earlier foils such as Fe, Cu, and Nb were also excited with the K x-rays of iodine. The values of $I_0 G\varepsilon$ obtained with the Fe, Cu, and Nb foils were then compared with the earlier set to get a normalization factor. With this normalization factor, the data of Ag, Cd, and In were then fitted with the earlier data and is shown in Fig. 3. The solid curve through the experimental points was used to obtain the values of the scattering cross sections. Also shown in this figure (dotted curve) is a theoretical curve obtained with the given specifications (Ge active layer, Ge dead layer, Be window thickness) of the detector and normalized to our experimental points. The nature of this curve is in good agreement with the measured $I_0 G\varepsilon$ values.

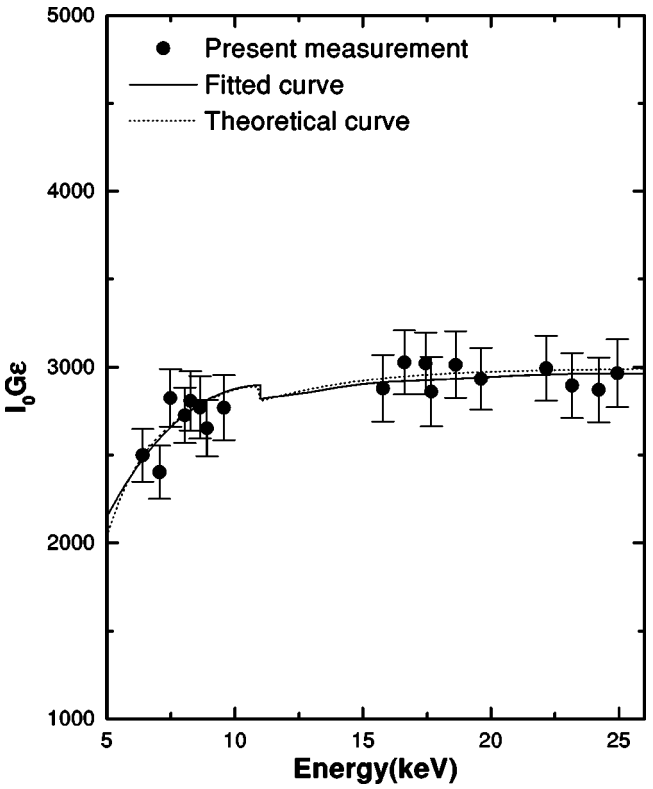

FIG. 3. The experimental values of $I_0 G\varepsilon$. The solid line (——) is drawn through experimental points and used to obtain the scattering cross sections. The broken line (---) is the theoretical fit.

III. DATA ANALYSIS

Although the elastic and inelastic peaks could be clearly identified in all the cases, it is not an easy task to find the latent contribution of the inelastic peak to the elastic ones. While the nature of the elastic peak is a Gaussian, it is not so for the inelastic peak. One therefore needs a good software to determine the intensity of the elastic peak. Here, we took the help of the PEAK FIT program [32] to obtain the peak integral. With a suitable background, any function like a Gaussian, a Lorentzian-Gaussian, an exponential Gaussian, or a Voigt function can be fitted with this program. With approximate initial values of the peak positions, widths, and shapes, the program automatically makes iterations to give the best fit of the interested region. For our present analysis, a linear background with a Gaussian function for the elastic peak and an exponential-Gaussian function for the inelastic peak were chosen. Figure 4 shows such a fitting for Fe and Pb where residual plots are also shown. In the region of the elastic peaks, the residuals are insignificant and the $r2$ values for the whole range was 0.98 signifying that the peak fitting was satisfactory. By slightly varying the shape of the background, we also tried to ascertain the maximum change in the elastic peak integral. The maximum change in intensity was $\leqslant 5\%$. As can be seen from Eq. (4), the errors in elastic scattering cross section propagate from (i) N_{el}, (ii) $I_0 G\varepsilon_{\mathrm{el}}$, (iii) m, and (iv) β. In the present experiment ΔN_{el} varies from 4–6 %, $\Delta I_0 G\varepsilon_{\mathrm{el}}$ is 5–7 %, Δm is 2%, and $\Delta\beta$ varies from 2–4 %. So the overall error in our scattering cross section varies between 8–10 %.

IV. RESULTS AND DISCUSSIONS

All the differential elastic scattering cross sections obtained in the present study are shown in Table III. Theoretical

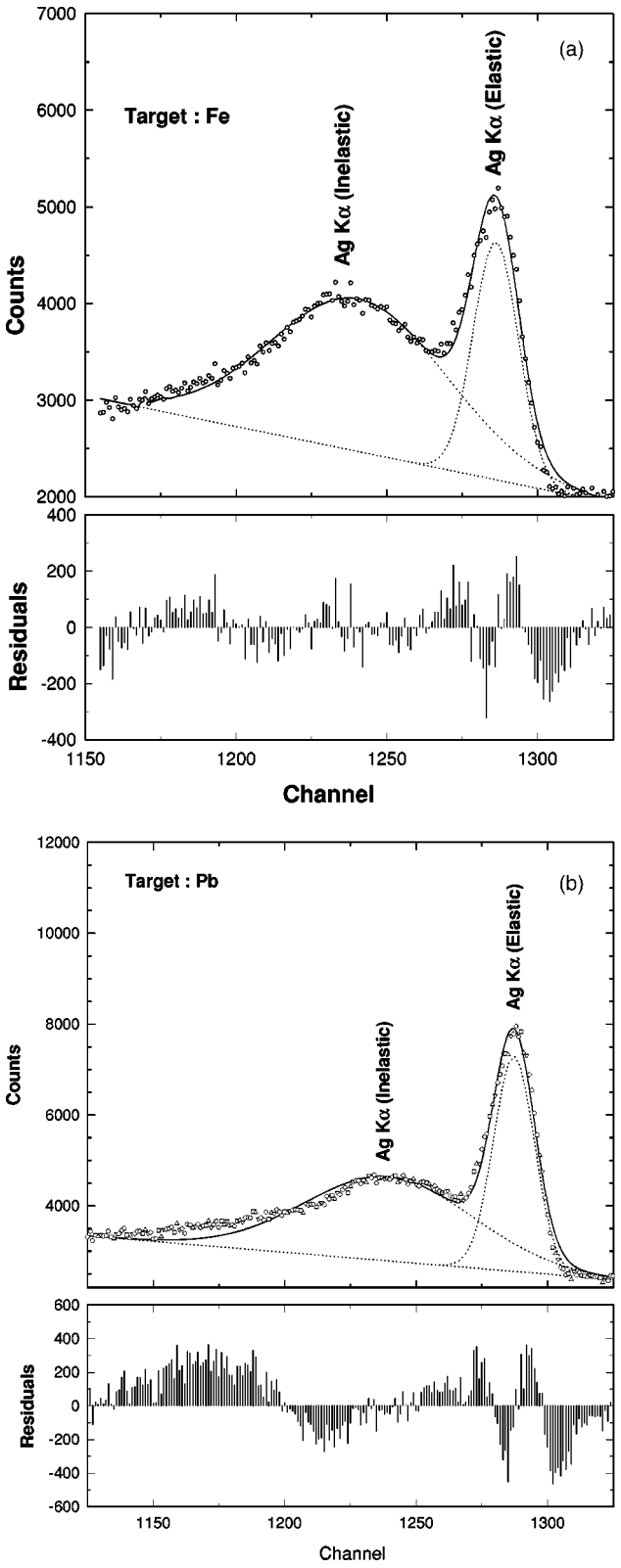

FIG. 4. Elastic and inelastic peaks fitted with the PEAK FIT program. The residual plots are also shown (a) for Fe, (b) for Pb.

predictions of the differential elastic scattering cross sections based on NFF, RFF, MRFF, relativistic form factor with anomalous scattering correction (RFFASF), modified relativistic form factor with anomalous scattering factor (MRFFASF), and the *S* matrix theories obtained from Ref. [33] are also shown in Table III. The percent deviations $[(\sigma_{\text{expt}}-\sigma_{\text{thet}})/\sigma_{\text{expt}}\times 100]$ of the present data from each of the above predictions are shown in Table IV. It is observed that the predictions of the RFFASF and MRFFASF from the data are almost the same and so is the case with the *S* matrix with the exception that the deviation is slightly less for the high *Z* elements. The predictions of the other two theories NFF and MRFF also deviate to the same extent from the present data. So for clarity of graphical representation of the present measurements, only the predictions of the NFF, RFF, and *S* matrix theory along with the present data have been shown in Fig. 5. From a critical look at this figure, one can divide our total range of *Z* into four groups.

(a) For the region $Z=22-40$, the experimental values are better represented by the *S* matrix (RFFASF, MRFFASF) than the NFF (MRFF) or RFF which can also be seen from Table IV.

(b) For $Z=41$, 42, and 46, whose *K* absorption edges (18.9986, 19.9995, and 24.3503 keV, respectively) are close to the exciting photon energy, the present experimental values are high compared to the theoretical predictions of *S*-matrix (RFFASF, MRFFASF). For $Z=42$, in particular, the measured values are about 30% higher than the *S* matrix calculation.

(c) For the next three *Z* ($Z=48$, 49, and 50) values, the deviation from the *S* matrix (RFFASF, MRFFASF) theory decreases but reverses its sign. For the NFF (MRFF) and RFF these deviations are larger.

(d) From $Z=62-82$, the average deviation of the data from the *S* matrix (RFFASF, MRFFASF) prediction was found to be higher than those of NFF (MRFF) and comparable to RFF.

A direct comparison of our measurements can be made only with the data of Bui and Milazzo [22] who had used the same exciting energy and scattering angle. Figure 6 shows such a comparison where it can be seen that except for Nb and Mo all their data agree very well with those of ours.

It is well known that near the absorption edges, anomalous scattering effects are observed. The most important part of our measurement is the *observation of the increase of scattering cross sections of* Nb *and* Mo *when compared with the most accepted and state-of-the-art S matrix calculations*. In this context, it would be relevant to have an idea of what results have already been observed by other groups near the *K* edges. Table V shows a few of such measurements done in the recent past. It is evident from Table V that near the *K* absorption edges either the data fit well with the *S* matrix calculation or lie below. In the year 1987, Kane *et al.* [34] had found that their data for Pb and Bi are 20–40 % higher when compared with the *S* matrix calculations but later in 1995 [35] they observed errors in their earlier experimental data and theoretical calculation and showed that the modified data fit well with the corrected calculations. In our present measurement, we have observed values that are higher by 30% for Mo and by 16% for Nb.

There are some other data available where either the ex-

TABLE III. Differential elastic scattering cross sections (*b*/atom) of the elements for 22.1-keV x rays at 90°.

Element (Z)	Expt. cross section (error)	Theoretical scattering cross sections calculated					
		NFF	RFF	RFFASF	MRFF	MRFFASF	S matrix
Ti (22)	0.86 (0.08)	0.830	0.866	0.948	0.852	0.950	0.938
V (23)	0.98 (0.09)	0.934	0.968	1.065	0.952	1.069	1.055
Fe (26)	1.39 (0.12)	1.208	1.240	1.384	1.215	1.389	1.370
Ni (28)	1.53 (0.13)	1.365	1.398	1.574	1.367	1.580	1.560
Cu (29)	1.67 (0.14)	1.441	1.477	1.667	1.442	1.674	1.652
Zn (30)	1.69 (0.15)	1.517	1.558	1.761	1.519	1.769	1.745
Zr (40)	3.19 (0.30)	3.068	3.262	3.186	3.150	3.204	3.165
Nb (41)	3.92 (0.35)	3.364	3.578	3.320	3.453	3.339	3.300
Mo (42)	4.74 (0.41)	3.689	3.924	3.386	3.785	3.406	3.365
Pd (46)	4.20 (0.37)	5.206	5.526	3.867	5.320	3.892	3.845
Cd (48)	4.90 (0.44)	6.045	6.390	5.057	6.144	5.089	5.019
In (49)	5.29 (0.48)	6.466	6.819	5.592	6.552	5.625	5.544
Sn (50)	5.82 (0.50)	6.879	7.238	6.101	6.949	6.137	6.045
Sm (62)	10.04 (0.93)	10.851	11.426	11.135	10.821	11.209	10.971
Gd (64)	10.85 (1.00)	11.482	12.139	11.977	11.466	12.058	11.792
Dy (66)	11.50 (1.08)	12.128	12.871	12.830	12.126	12.921	12.629
Er (68)	12.25 (1.13)	12.824	13.684	13.758	12.860	13.858	13.537
Yb (70)	13.08 (1.23)	13.599	14.578	14.751	13.668	14.862	14.510
Au (79)	18.40 (1.66)	19.054	20.654	20.829	19.200	20.992	20.468
Pb (82)	20.79 (1.83)	21.683	23.431	23.252	21.731	23.433	22.853

citation energies or the scattering angles are very similar to ours. Shahi *et al.* [14] measured the differential elastic scattering cross sections for 30 elements ($12 \leqslant Z \leqslant 92$) for 22.1 keV at an angle of 117° using an annular Cd radioisotope. They observed that theoretical values based on *S* matrix and MRFFASF are, on the average, higher by 9% and 12%, respectively, from the data. In a similar measurement the same group [36] measured the scattering cross sections of elements $13 \leqslant Z \leqslant 82$ at 130° for 59.54 keV using an annular Am radioactive source. Although their data were always less than the NFF, MRFF, and *S* matrix calculations, they showed that the NFF prediction gives better results for low and medium *Z* elements compared to MRFF and *S* matrix. For heavy elements, the *S* matrix calculations showed good agreement. Elyaseery *et al.* [15] measured the cross sections for the elements Cu, Zn, Zr, Nb, Mo, Ag, Cd, In, Sn, Ta, and W using an annular Am source at 145°, 154°, and 165° for the energies 13.95, 17.75, 26.36, and 59.54 keV. They compared their data with the RFF, MRFF, RFFASF, and MRFFASF. They observed that RFFASF predictions provided the best

TABLE IV. The percent deviation $[(\sigma_{expt}-\sigma_{theo})/\sigma_{expt}\times 100]$ of the present data from different theoretical models.

Element (*Z*)	NFF	RFF	RFFASF	MRFF	MRFFASF	*S* matrix
Ti (22)	3	−1	−10	1	−10	−9
V (23)	5	1	−9	3	−9	−8
Fe (26)	13	11	0	12	0	1
Ni (28)	11	9	−3	11	−3	−2
Cu (29)	14	12	0	14	0	1
Zn (30)	10	8	−4	10	−5	−3
Zr (40)	4	−2	0	1	0	1
Nb (41)	14	9	15	12	15	16
Mo (42)	22	17	29	20	28	29
Pd (46)	−24	−31	8	−27	7	8
Cd (48)	−23	−30	−3	−25	−4	−2
In (49)	−22	−29	−6	−24	−6	−5
Sn (50)	−18	−24	−5	−19	−5	−4
Sm (62)	−8	−14	−11	−8	−12	−9
Gd (64)	−6	−12	−10	−6	−11	−9
Dy (66)	−5	−12	−12	−5	−12	−10
Er (68)	−5	−12	−12	−5	−13	−11
Yb (70)	−4	−11	−13	−4	−14	−11
Au (79)	−4	−12	−13	−4	−14	−11
Pb (82)	−4	−13	−12	−5	−13	−10

agreement with the experimental results. Garg *et al.* [16] measured the elastic cross sections of C, Si, V, Fe, Cu, Zn, Mo, Au, and Pb with a secondary target excited system. The exciting radiation was 34.60 keV while the angle of measurement was 90°. Using the RFF and MRFF formalism, they calculated the normalized integrated differential cross section and observed that experimental values are 20–50 % higher than the theoretical predictions. They also compared their data with Tirsell, Slivinsky, and Ebert [17] who using an x-ray fluorescence (XRF) setup had measured the cross sections of Sn, Sm, Ta, Pt, and Au at angles 45° to 135° in the energy range 25–75 keV. In their paper, Garg *et al.* showed that the data of Tirsell, Slivinsky, and Ebert showed the same trend as that of theirs. Rao, Cesareo, and Gigante [18] mea-

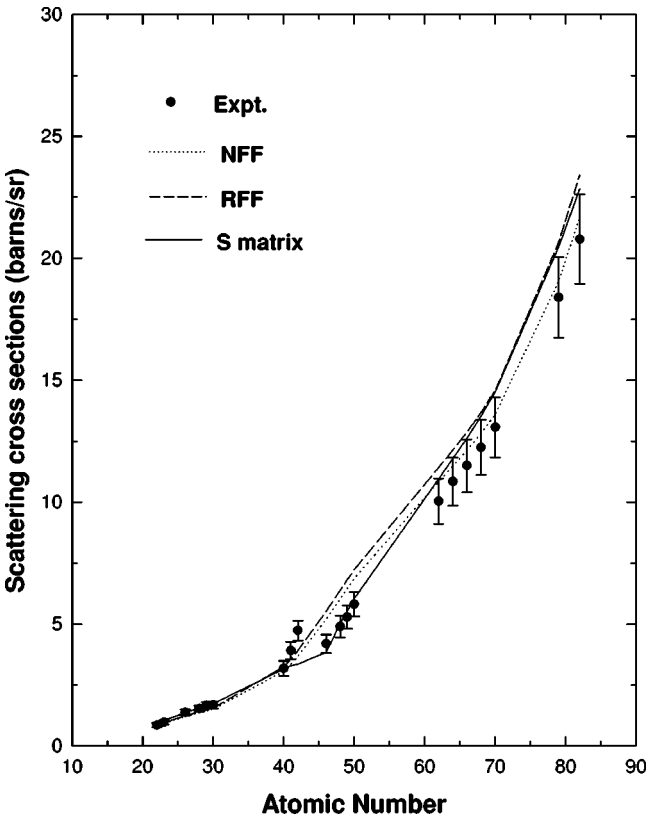

FIG. 5. Present data (●) are plotted along with the predictions of the nonrelativistic form factor (NFF, ····), relativistic form factor (RFF, ---), and *S* matrix (——) calculations.

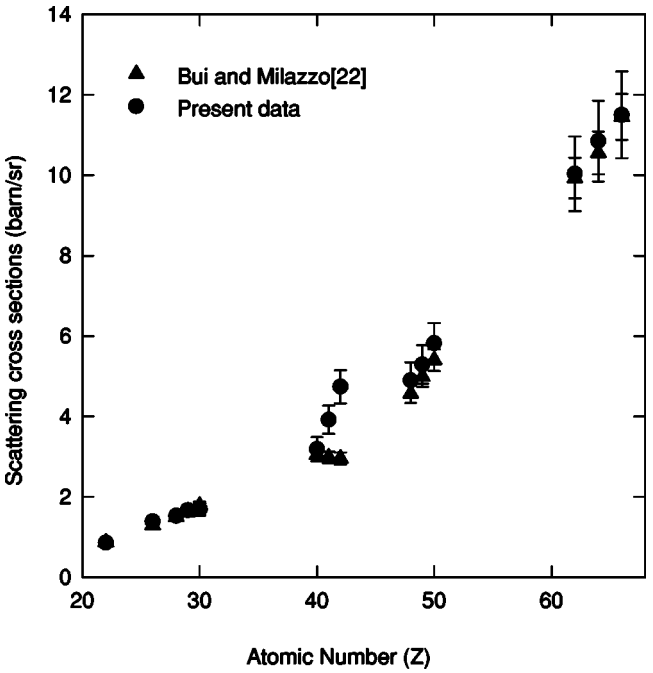

FIG. 6. Comparison of the present data (●) with those of Bui and Milazzo (▲) [22] (an error of 5% was assigned to the data of Ref. [22]).

TABLE V. Some measurements near the *K* absorption edges.

Exciting energy (keV)	Angle (deg)	Elements having *K* edge near the exciting radiation	Binding energy (keV)	Reference	Compared to *S* matrix calculation
88.03	125	Pb	88.00	Kane [34]	Higher
		Bi	90.53		
88.03	125	Pb	88.00	Basavaraju [35]	Good agreement
		Bi	90.53		
59.5	130	Dy	53.79	Puri [36]	Less
59.5	60–150	Er	57.49	Ghose [37]	Less
		Yb	61.33		
59.5	60–120	Er	57.49	Baraldi [38]	Good agreement
		Yb	61.33		
22.16	117	Nb	18.97	Shahi [14]	Less
		Mo	20.00		
22.16	90	Nb	18.97	Bui [22]	Less
		Mo	20.00		
21.2–43.7	60–120	Xe	34.56	Smend [20]	Good agreement

sured the cross sections of Al, Cu, Sr, Cd, Ce, Pr, Sm, Pt, Au, and Pb at 90° with 14.93, 17.44, and 21.12 keV. They used a secondary target excited XRF setup. The data were compared with the theoretical predictions of NFF, RFF, and MRFF. It was observed that MRFF gave better results compared with the other theories. In a latter paper [19] they also measured the scattering cross section for Pt at 23.10, 24.14, 25.20, 26.27, and 32.06 keV using the same setup. Data were always higher than NFF, RFF, and MRFF by 13–17 %, 8–10 %, and 14–16 %, respectively. Smend *et al.* [20] using the synchrotron beam measured the scattering cross sections of Kr and Xe from 21.2 to 43.7 keV at 60°, 90°, and 120°. Experimental values agreed well with the *S* matrix, RFFASF, and MRFFASF even near the *K* edges of Xe. Only at smaller and larger photon energies, the difference between the experiment and theory were comparable to or slightly larger than the experimental error.

From a comparison of the present data with the theoretical predictions one finds the following.

(a) For the low *Z* elements ($Z=22-40$) the present data are in general higher ($\sim$7%) than the predictions of NFF, RFF, MRFF but lower ($\sim$3%) than the RFFASF, MRFFASF, and *S* Matrix predictions.

(b) For elements ($Z=41$, 42, and 46) having *K* edges close to the excitation energy, the data are always high compared to any existing theories. For $Z=42$ where the difference between the *K* absorption edge and the exciting radiation is the minimum ($\sim$2.1 keV) the cross section values are almost 30% higher than the *S* matrix calculations and for $Z=41$ this factor is $\sim$ 16%. For $Z=46$, the experimental value is 25% lower than the predictions of NFF (MRFF) and RFF but higher by 8% than the *S* matrix (RFFASF, MRFFASF) calculations. As suggested by Jung *et al.* [21] this mismatch of the measured elastic scattering cross sections with the *S* matrix predictions near the *K* absorption edges might be due to the nonlocal exchange effect and electron correlation which have not been included in the *S* matrix calculation. These authors had measured the ratio of elastic and total cross sections of Ne and He at 11, 15, 18, and 22 keV at 90° and concluded that none of the current theories could properly describe the scattering in Ne and also advocated the inclusion of correction factors for the above two effects in the theoretical calculations.

(c) For $Z=48$, 49, and 50, the data are lower by 4% than the predictions of *S* matrix (RFFASF, MRFFASF) and 22% lower than those of NFF (MRFF) and RFF.

(d) For high *Z* elements ($Z=62-82$) our data are closer to the predictions of NFF (MRFF) (lower by 5%) and this deviation increases to 11% when compared with other theories.

Systematically lower values of the data for these elements, as seen from Fig. 5, cannot be explained due to the loss of counts arising from high count rates as was mentioned by Bradley, Goncalves, and Kane [13] in connection with the measurements of Refs. [14,15,36]. In the present measurement the count rates for this region of *Z* varied between 600/s to 1100/s and so the possibility of loss of counts due to high count rates does not arise. At this moment, however, we are not in a position to offer any explanation for such behavior of the data.

V. CONCLUSION

Except for Nb, Mo, and Pd, the measured cross sections are always lying (within 10%) below the *S* matrix calculations. *For* Nb, Mo, *and* Pd *the cross sections are 16%, 29%, and 8% higher, respectively, than the S matrix calculations.* This difference in cross sections may signify the necessity of inclusion of some correction factors in the theoretical calculations.

ACKNOWLEDGMENTS

The authors are grateful to Professor P. Sen for his encouragement during the course of this work. Technical help from P. K. Das is also gratefully acknowledged.

[1] J. H. Hubbell, Wm. J. Veigele, E. A. Briggs, R. T. Brown, D. T. Cromer, and R. J. Howerton, J. Phys. Chem. Ref. Data **4**, 471 (1975); **6**, 615(E) (1977).
[2] J. H. Hubbell and I. Øverbø, J. Phys. Chem. Ref. Data **8**, 69 (1979).
[3] D. Schaupp, M. Schumacher, F. Smend, P. Rullhusen, and J. H. Hubbell, J. Phys. Chem. Ref. Data **12**, 467 (1983).
[4] D. T. Cromer and D. A. Liberman, J. Phys. Chem. **53**, 1891 (1970).
[5] D. T. Cromer and D. A. Liberman, Acta Crystallogr., Sect. A: Cryst. Phys., Diffr., Theor. Gen. Crystallogr. **A37**, 267 (1981).
[6] B. Henke, P. Lee, T. J. Tanaka, R. L. Shimabukuro, and B. K. Fujikawa, At. Data Nucl. Data Tables **27**, 1 (1982).
[7] B. L. Henke, E. M. Gullikson, and J. C. Davis, At. Data Nucl. Data Tables **54**, 181 (1993).
[8] G. E. Brown and D. F. Meyers, Proc. R. Soc. London, Ser. A **227**, 51 (1951).
[9] W. R. Johnson and K. T. Cheng, Phys. Rev. A **13**, 692 (1976).
[10] L. Kissel, R. H. Pratt, and S. C. Roy, Phys. Rev. A **22**, 1970 (1980).
[11] P. P. Kane, L. Kissel, R. H. Pratt, and S. C. Roy, Phys. Rep. **140**, 75 (1986).
[12] S. C. Roy, L. Kissel, and R. H. Pratt, Radiat. Phys. Chem. **56**, 3 (1999).
[13] D. A. Bradley, O. D. Goncalves, and P. P. Kane, Radiat. Phys. Chem. **56**, 125 (1999).
[14] J. S. Shahi, S. Puri, D. Mehta, M. L. Garg, N. Singh, and P. N. Trehan, Phys. Rev. A **55**, 3557 (1997).
[15] I. S. Elyaseery, A. Shukri, C. S. Chong, A. A. Tajuddin, and D. A. Bradley, Phys. Rev. A **57**, 3469 (1998).
[16] M. L. Garg, R. R. Garg, F. Hennrich, and D. Heimermann, Nucl. Instrum. Methods Phys. Res. B **73**, 109 (1993).
[17] K. G. Tirsell, V. W. Slivinsky, and P. J. Ebert, Phys. Rev. A **12**, 2426 (1975).
[18] D. V. Rao, R. Cesareo, and G. E. Gigante, Phys. Scr. **55**, 305 (1997).
[19] D. V. Rao, R. Cesareo, and G. E. Gigante, Phys. Scr. **50**, 314 (1994).
[20] F. Smend, D. Schaupp, H. Czerwinski, M. Schumacher, A. H. Millhouse, and L. Kissel, Phys. Rev. A **36**, 5189 (1987).
[21] M. Jung, R. W. Dunford, D. S. Gemmell, E. P. Kanter, B. Kraessig, T. W. LeBrun, S. H. Southworth, L. Young, J. P. L. Carney, L. LaJohn, R. H. Pratt, and P. M. Bergstrom, Jr., Phys. Rev. Lett. **81**, 1596 (1998).
[22] C. Bui and M. Milazzo, Nuovo Cimento **11**, 655 (1989).
[23] D. Mitra, M. Sarkar, and D. Bhattacharya, Radiat. Phys. Chem. **58**, 119 (2000).
[24] A. C. Mandal, M. Sarkar, D. Bhattacharya, and P. Sen, Nucl. Instrum. Methods Phys. Res. B **174**, 41 (2001).
[25] R. D. Giaque, R. B. Garrett, and L. Y. Goda, Anal. Chem. **51**, 511 (1979).
[26] P. P. Kane, Radiat. Phys. Chem. **50**, 31 (1997).
[27] M. Sarkar and M. L. Garg, Nucl. Instrum. Methods Phys. Res. B **83**, 373 (1993).
[28] M. J. Berger and J. H. Hubbell, NBS Report No. NBSIR-87-3597 (1987).
[29] J. H. Scofield, Lawrence Livermore Laboratory Report No. UCRL-51326 (1973).
[30] M. O. Krause, J. Phys. Chem. Ref. Data **8**, 307 (1979).
[31] S. I. Salem, S. L. Panossian, and R. A. Krause, At. Data Nucl. Data Tables **14**, 91 (1974).
[32] PEAK FIT, Jandel Scientific, Version 4. 1991.
[33] Internet address, http://www.phys.llnl.gov/Research/scattering/index.html
[34] P. P. Kane, G. Basavaraju, S. M. Lad, K. M. Varier, L. Kissel, and R. H. Pratt, Phys. Rev. A **36**, 5626 (1987).
[35] G. Basavaraju, P. P. Kane, S. M. Lad, L. Kissel, and R. H. Pratt, Phys. Rev. A **51**, 2608 (1995).
[36] S. Puri, B. Chand, D. Mehta, M. L. Garg, N. Singh, and P. N. Trehan, Nucl. Instrum. Methods Phys. Res. B **111**, 209 (1996).
[37] S. K. Ghose, M. Ghose, S. S. Nandi, A. C. Nandi, and N. Choudhuri, Phys. Rev. A **41**, 5859 (1990).
[38] C. Baraldi, E. Casnati, A. Tartari, M. Andreis, and B. Singh, Phys. Rev. A **54**, 4947 (1996).